Commissioning of High Efficiency Standing Wave Linac for Industrial Applications

A.N. Ermakov[a,b], V.V. Khankin[a,b], A.S. Alimov[a,b], V.V. Klementiev[b], L.Yu. Ovchinnikova[a,b], N.I. Pakhomov [a,b], Yu.N. Pavshenko[b], A.S. Simonov[b], N.V. Shvedunov[a,b], V.I. Shvedunov[a,b]

[a)]Skobeltsyn Institute of Nuclear Physics, Lomonosov Moscow State University

[b)]Laboratory of Electron Accelerators MSU, Ltd.

Leninskie Gory, 119992 Moscow, Russia

MSU ELECTRON ACCELERATORS

- 1959-1984 – Photonuclear reactions study with 35 MeV betatron
- 1985-1992 – 175 MeV race track microtron project
  6.7 MeV CW injector built
- 1992-1996 – several 1- 2 MeV high power CW accelerators built
- 1996-2001 – 70 MeV pulsed race track microtron built
- 1998-2003 – 35 MeV high brightness beam accelerator built
- 1999-2001 – 60 kW, 1.2 MeV compact CW linac built
- 2000-now – Vacuum laser acceleration theoretical and experimental study
- 2003-2007 – 50 kW, 10 MeV technological linac
- 2003-2010 – 55 MeV pulsed race track microtron built
- 2007-present time – 3/6 MeV linac with pulse to pulse energy switch for cargo inspection built
- 2009-present time – 3-8 MeV industrial linac for ROSATOM plants
- 2013 –present time – 15 kW, 10 MeV technological linac for sterilization plants

Initial Approximation

Z_{eff} = 70 – 90 MOm/m Linac length L = 1,25 m

For relativistic beam $L = \frac{E^2}{Z_{eff} q \overline{P_W}}$

$$P_W = q\overline{P_W} = 1.14\ MW$$

Klystron KIU-147A $q = {P_{kl}}/{\overline{P_{kl}}} = \frac{6000\ kW}{25\ kW} = 240$

$$\overline{P_W} = 5\ kW, I = 430\ mA$$

$$\eta = \overline{P_b}/(\overline{P_b} + \overline{P_W}) \cdot 100\% = 75\% \quad P_b = E \cdot I = 4.3\ MW$$

$$\beta = 1 + P_b/P_W = 4.77$$

Linac description

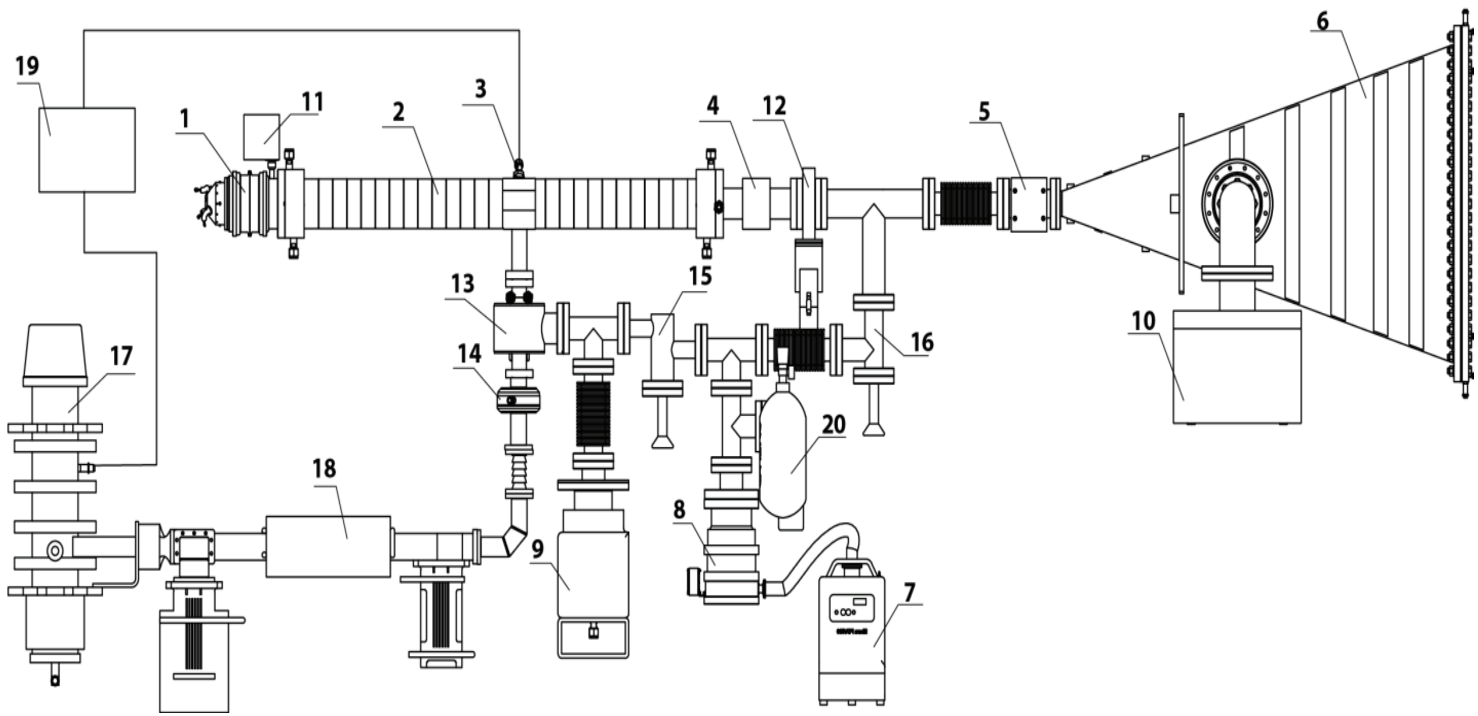

Figure 1: Linac structural. 1 – e-gun, 2 – SW cavity, 3 – RF loop, 4 – beam current monitor, 5 – scanning dipole magnet, 6 – scan vacuum chamber, 7 – backing pump, 8 – turbomolecular pump, 9, 10, 11 – ion pumps, 12 – gate valve, 14 – RF vacuum window, 15, 16 – vacuum valves, 17 – klystron, 18 – RF ferrite isolator, 19 – low RF power unit, 20 – insulating gas tank.

Linac description

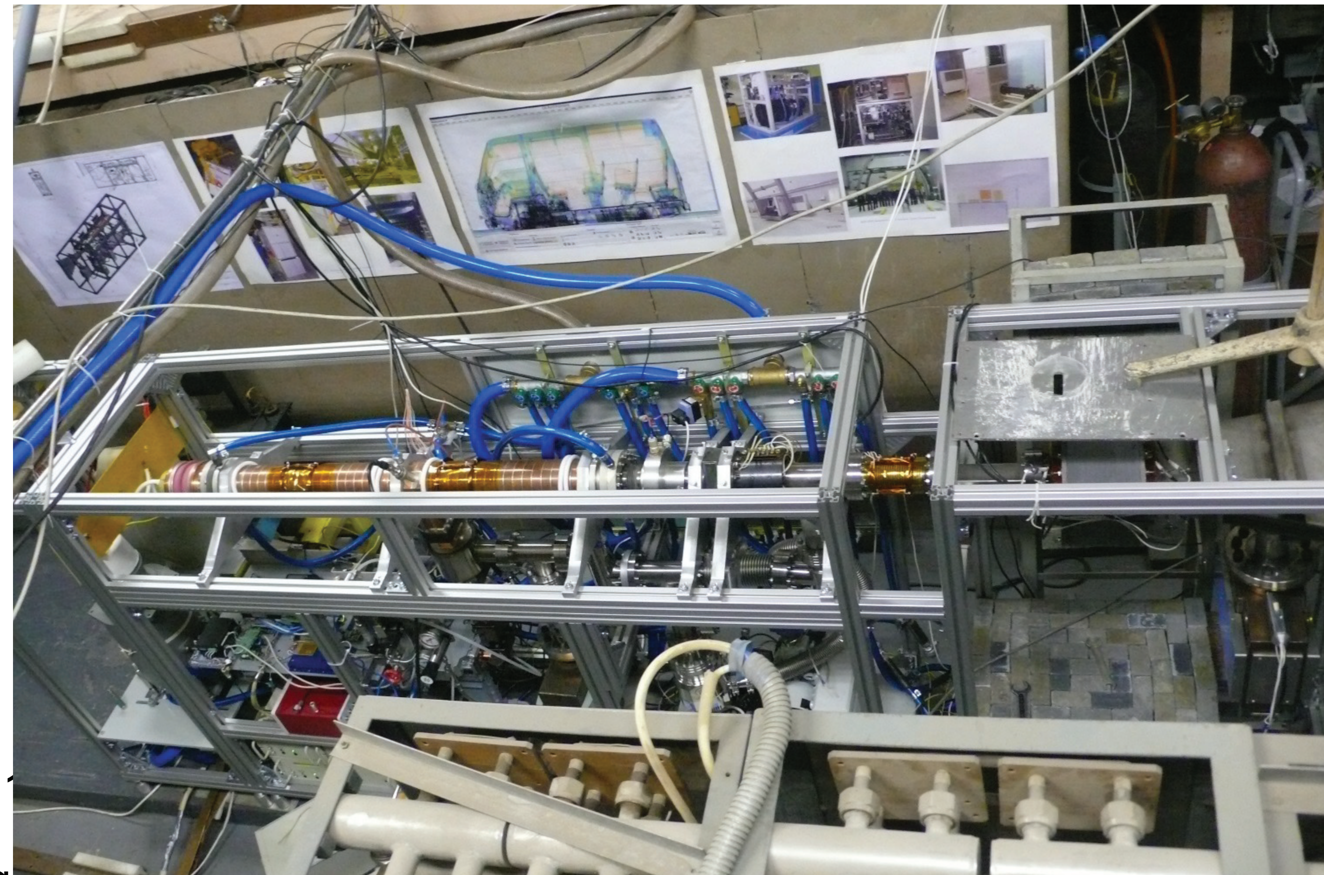

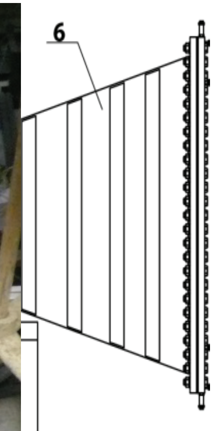

Figure … 4 – beam current … mber, 7 – backing pump, 8 – turbomolecular pump, 9, 10, 11 – ion pumps, 12 – gate valve, 14 – RF vacuum window, 15, 16 – vacuum valves, 17 – klystron, 18 – RF ferrite isolator, 19 – low RF power unit, 20 – insulating gas tank.

Accelerating structure

- 24 accelerating and 23 coupling cells
- 1st accelerating cell – a pre-buncher
- > 60% capture efficiency
- High vacuum conductivity
- 210 kW/m power dissipation density in the cavity walls

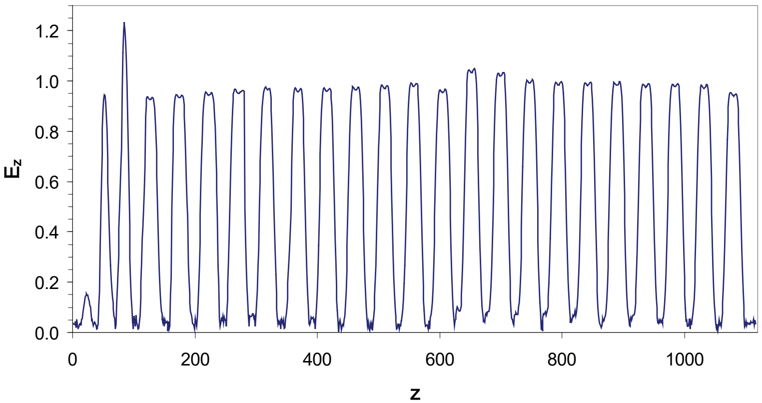

Figure 2: On-axis field distribution.

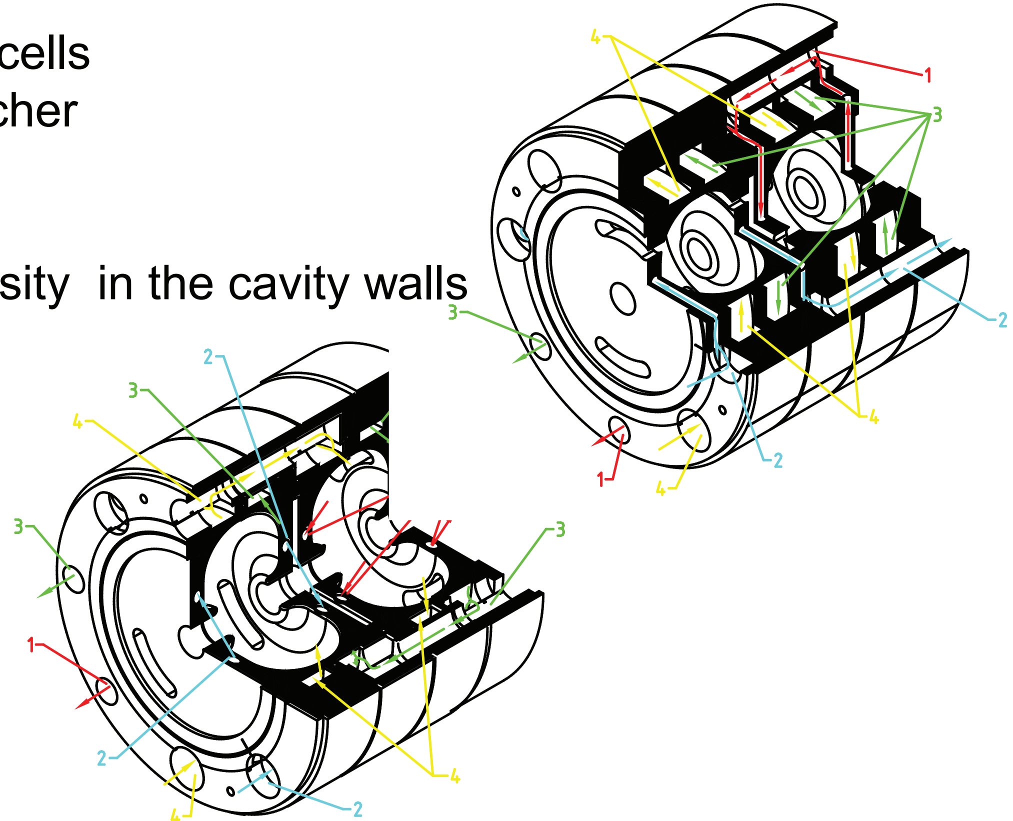

Figure 3: Channels of cavity cooling.

RF System

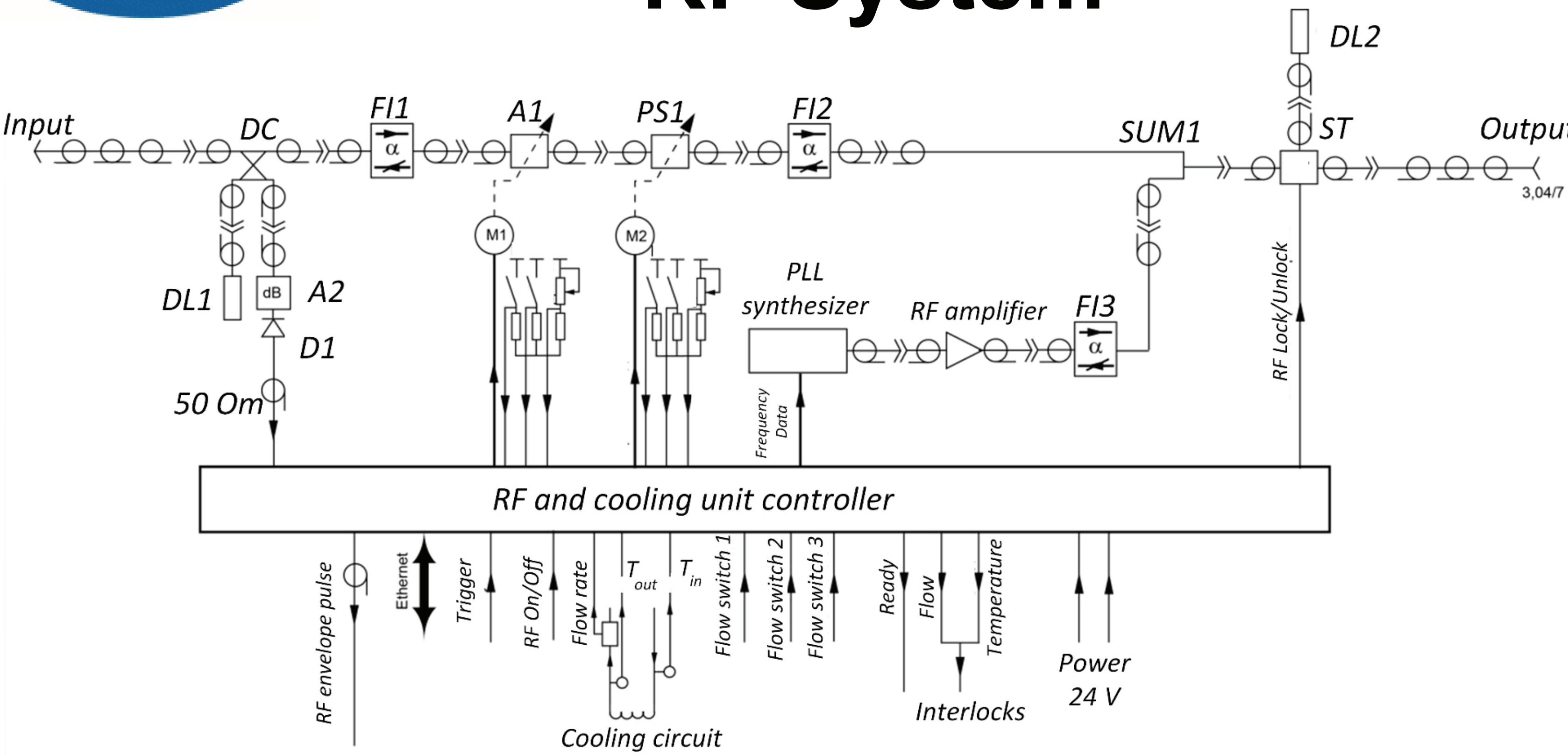

Figure 4: Low RF power unit. DC – directional coupler, DL1, DL2 – dummy loads, D1 – RF diode, A2 – coaxial attenuator, FI1 – FI3 – ferrite isolators, A1 – variable attenuator, PS1 – variable phase shifter, SUM1 – RF power summer, ST – RF stopper, M1, M2 – controlled motors with position sensors.

Electron Gun HV supply

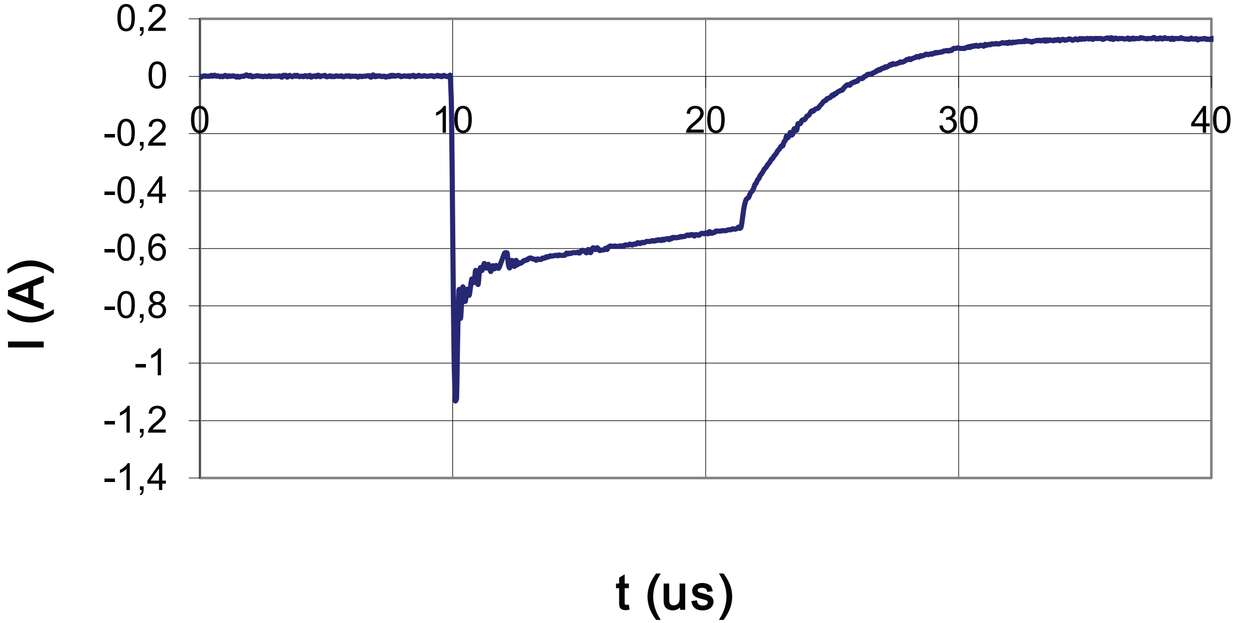

Figure 5: E-gun beam envelope.

Figure 6: E-gun HV unit.

Cathode voltage	**- 50 kV**
Cathode voltage instability	**<0,1 %**
Power consumption	**250 W**
Intermediate electrode voltage	**+ 2..+15 kV**
E-gun beam current (pulsed)	**-200..-900 mA**

Klystron KIU-147A HV supply

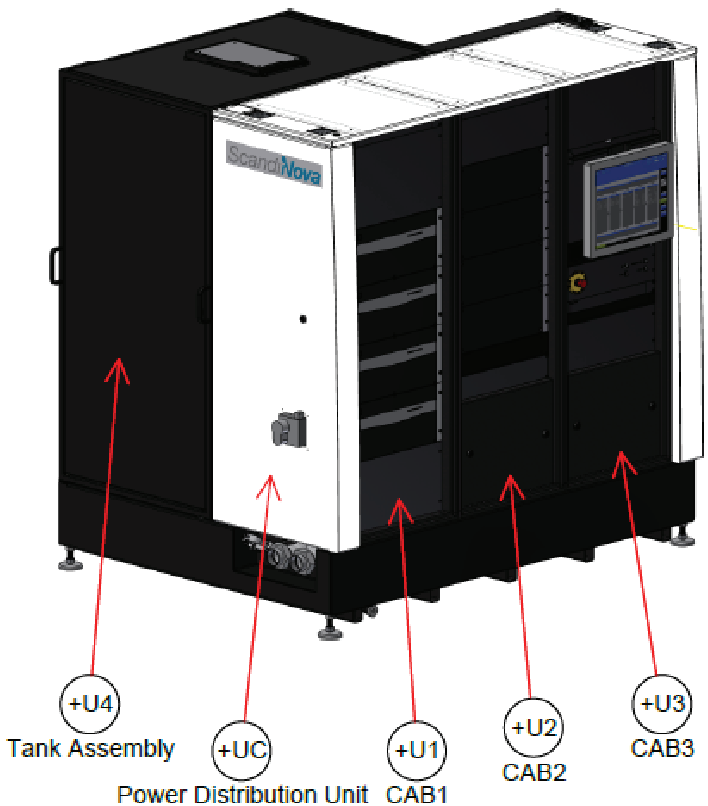

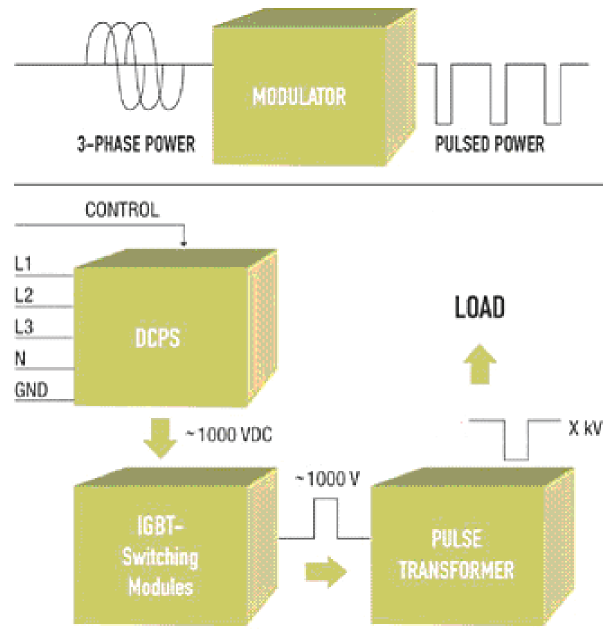

Figure 8: Modulator block diagram.

Figure 7: K2 Solid State Modulator based on The Split Core™ technology and Parallel Switching™ (**ScandiNova Systems AB Company, Sweden)**.

.

Beam energy and power measurements

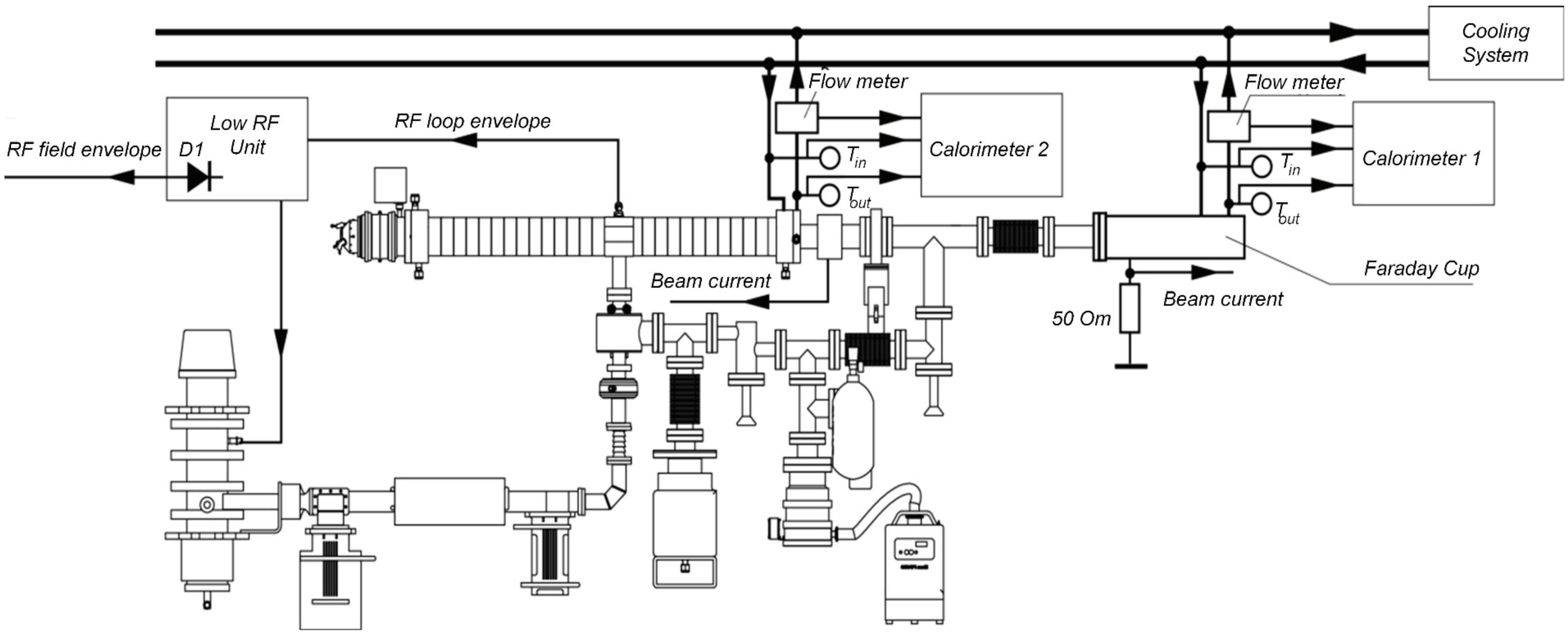

Figure 9: Average energy and beam power measurements circuit.

$$\bar{E} = \int_0^{E_{max}} Ef(E)dE, \quad \int_0^{E_{max}} f(E)dE = 1 \qquad \bar{E} = \bar{P}/\bar{I}$$

$$\bar{I} = I \times \tau \times f_{rep} \qquad \tau = 6 \ldots 15\ \mu s$$

SINP MSU

Beam energy and power measurements

a)

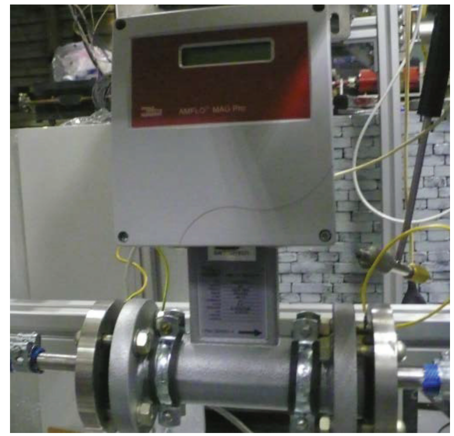

b)

c)

Figure 10: (a) Faraday cup and temperature sensors PLH 100/105 CE M,
(b) Flow meter AMFLO MAG Pro DN25 PN16 PP,
(c) Calorimeters Controller ENERGY Master–101-Prot-AC.

Beam energy and power measurements

a)

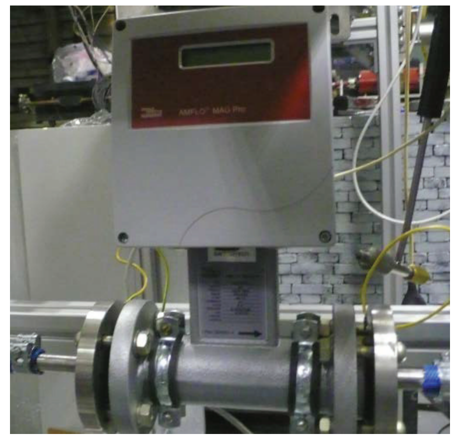

b)

c)

Figure 10: (a) Faraday cup and temperature sensors PLH 100/105 CE M,
(b) Flow meter AMFLO MAG Pro DN25 PN16 PP,
(c) Calorimeters Controller ENERGY Master–101-Prot-AC.

Beam energy and power measurements

a)

b)

c)

Figure 10: (a) Faraday cup and temperature sensors PLH 100/105 CE M,
(b) Flow meter AMFLO MAG Pro DN25 PN16 PP,
(c) Calorimeters Controller ENERGY Master–101-Prot-AC.

Beam energy and power measurements

Table 1: CALEC® Energy Master uncertainties.

Temperatures difference (K)	Measurement uncertainties
3	0,7%
6	0,3%
20	0,07%
100	0,02%

Table 2: Required flow of cooling water and average beam power for 0,7% uncertainty.

Average beam power, kW	Cooling liquid flow, l/min
1	$\leq$ 4,8
5	$\leq$ 24
10	$\leq$ 48
15	$\leq$ 72

Beam energy and power measurements

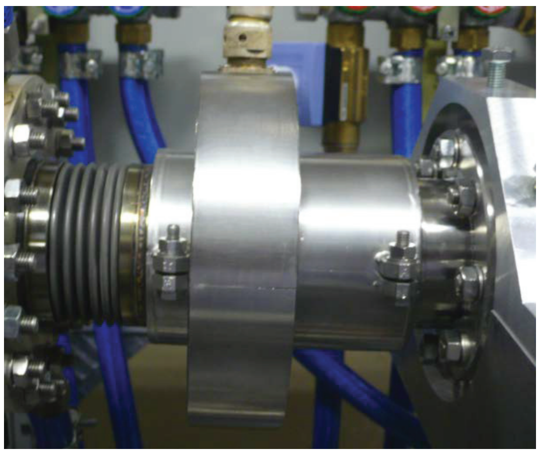

a)

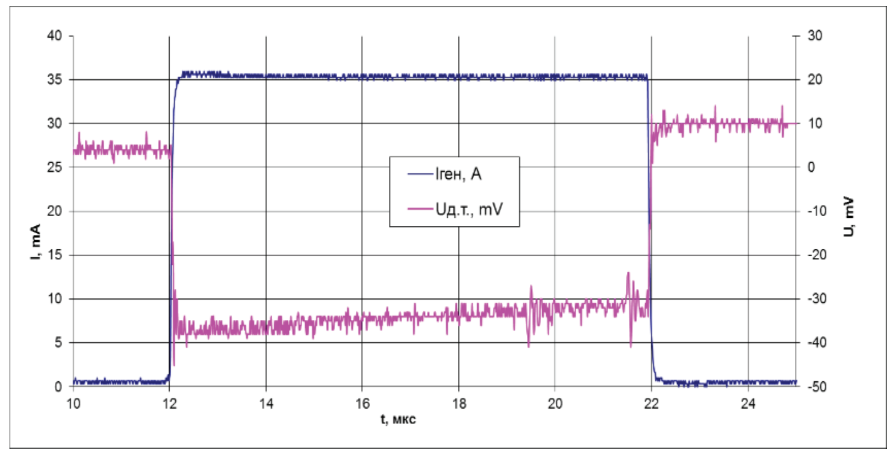

b)

Figure 11: (a) Beam current monitor, (b) Calibration current pulse (blue curve) and output voltage pulse of BCM.

Beam energy and power measurements

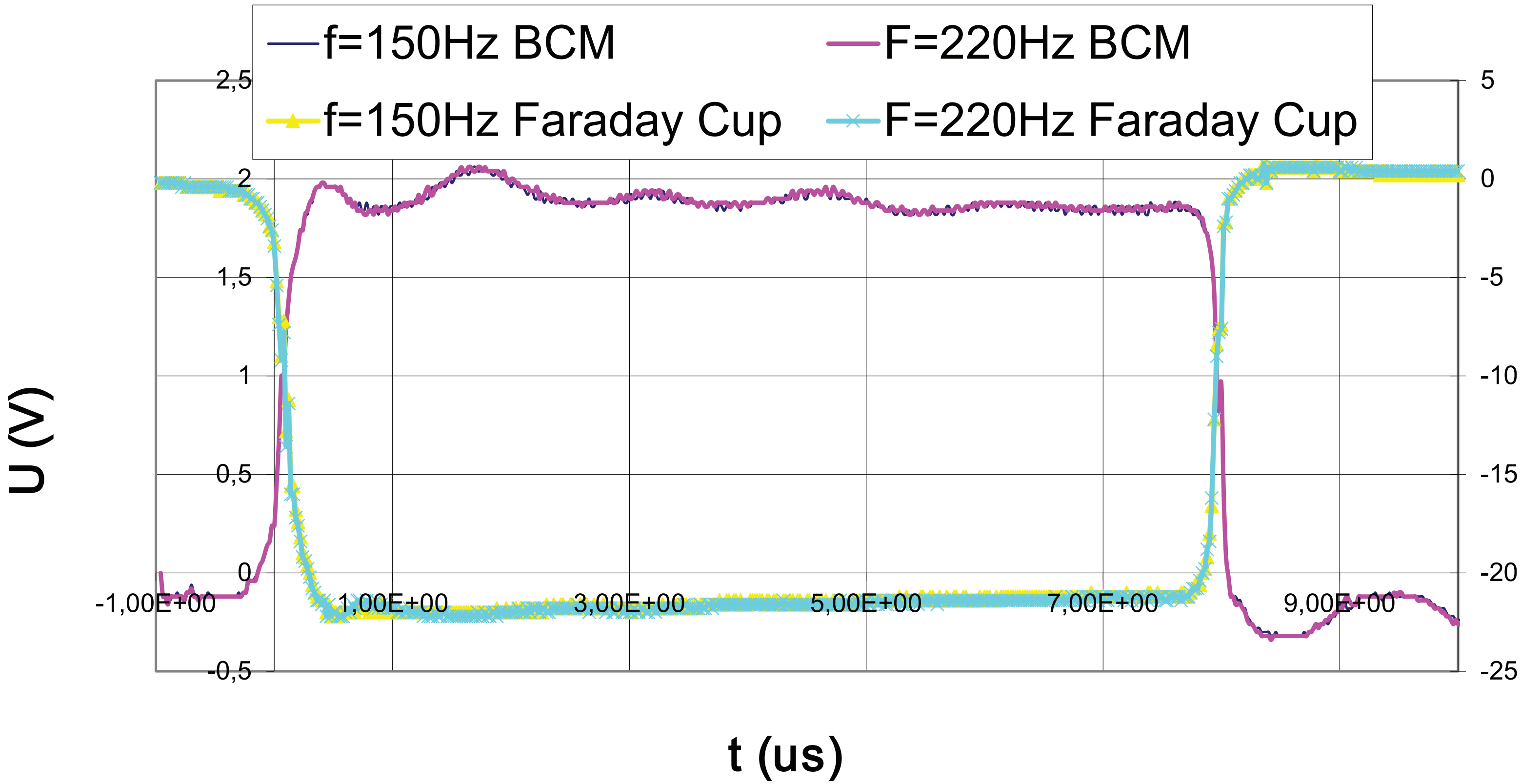

Figure 12: Beam current envelopes from BCM sensor and Faraday Cup.

Beam energy and power measurements

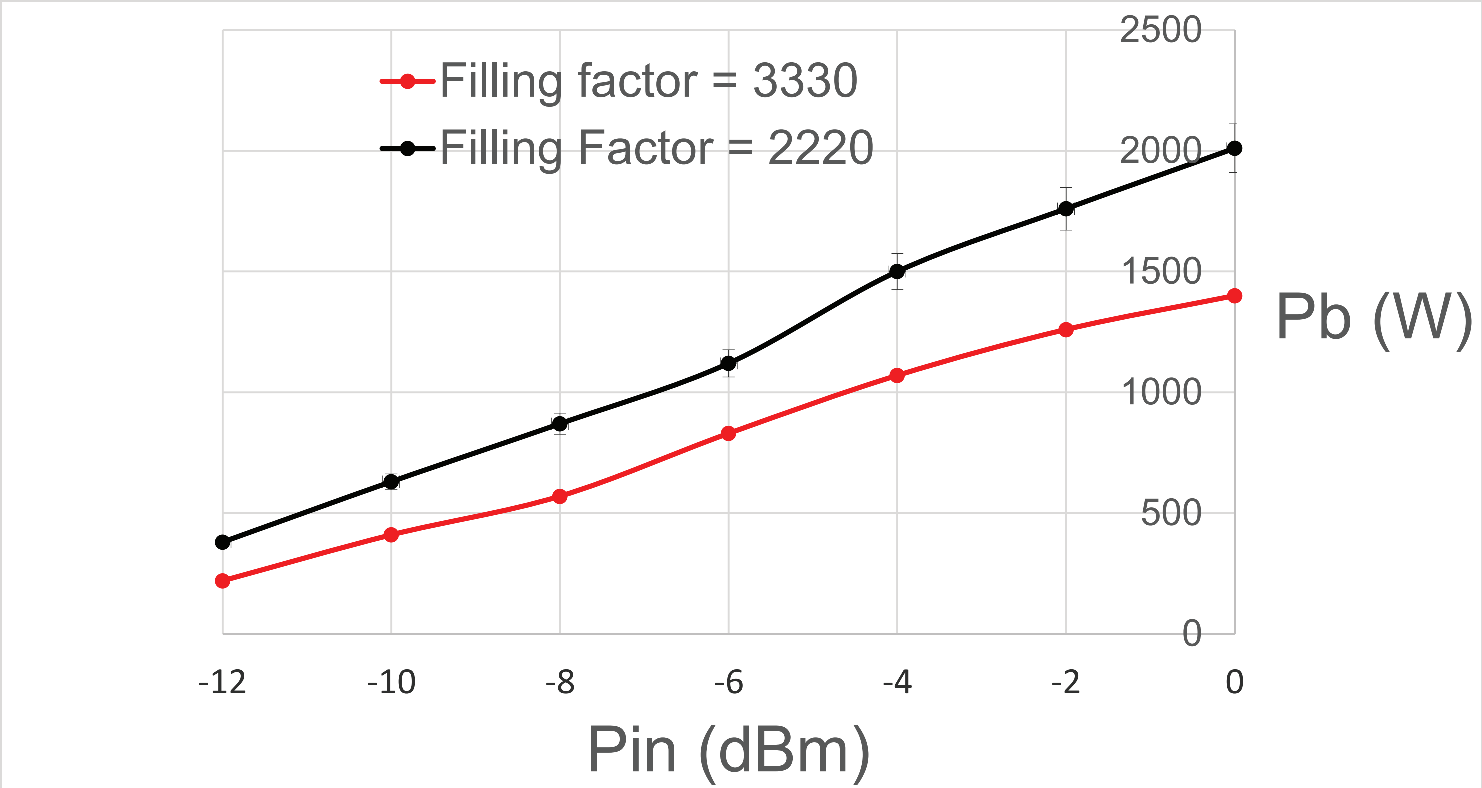

Figure 13: Dependence on the average beam power from output power of RF synthesizer.

Beam energy and power measurements

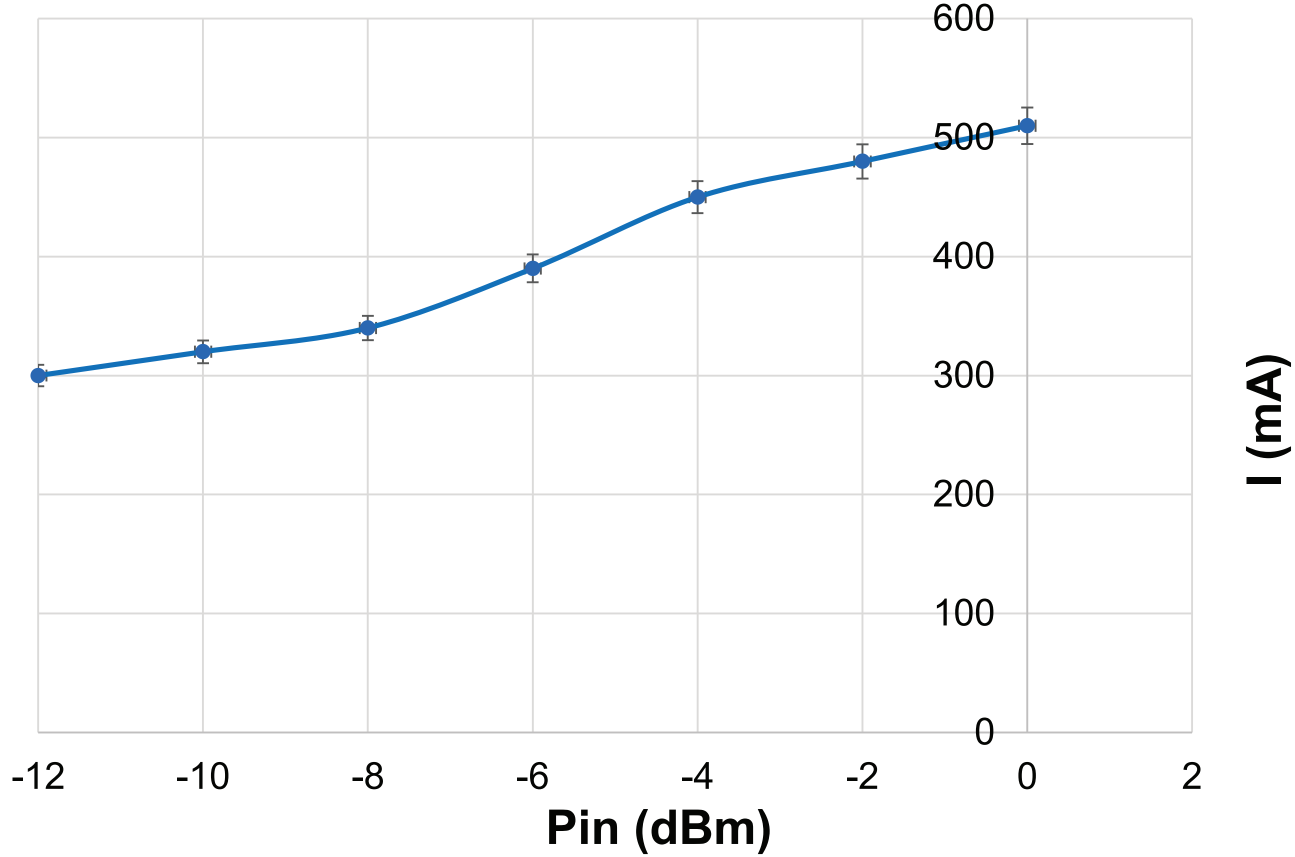

Figure 14: Dependence on the pulsed beam current from output power of RF synthesizer.

Beam energy and power measurements

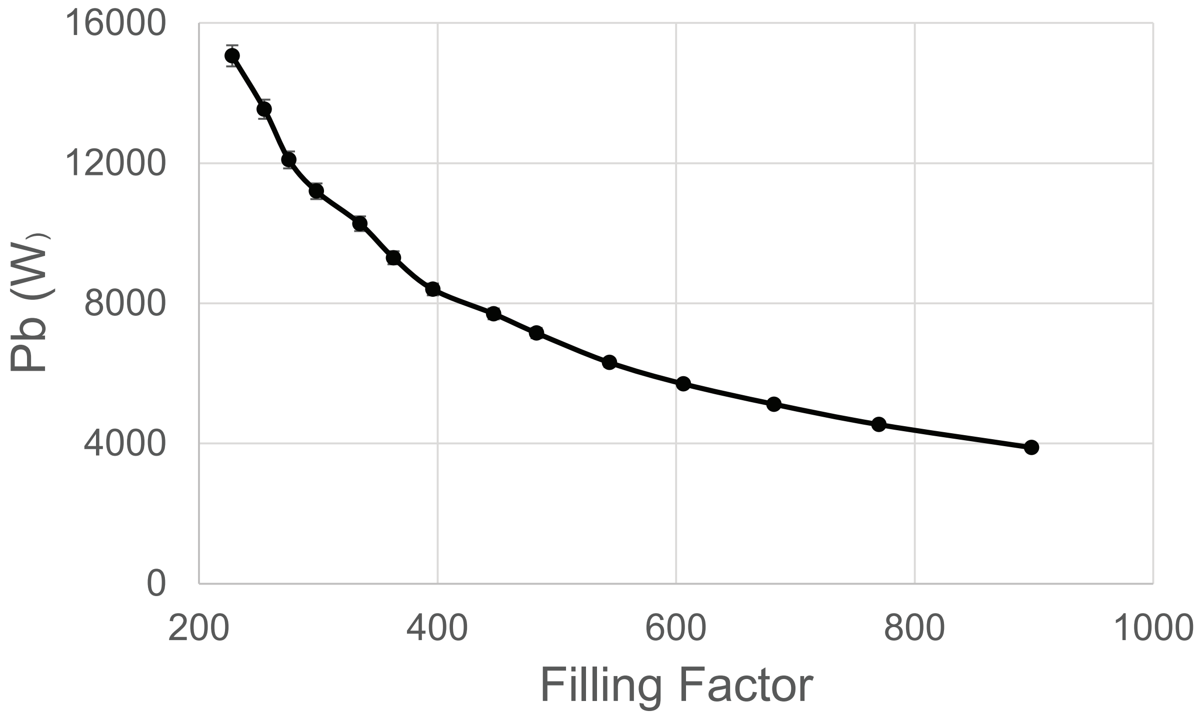

Figure 15: Dependence on the average beam power from filling factor.

Beam energy and power measurements

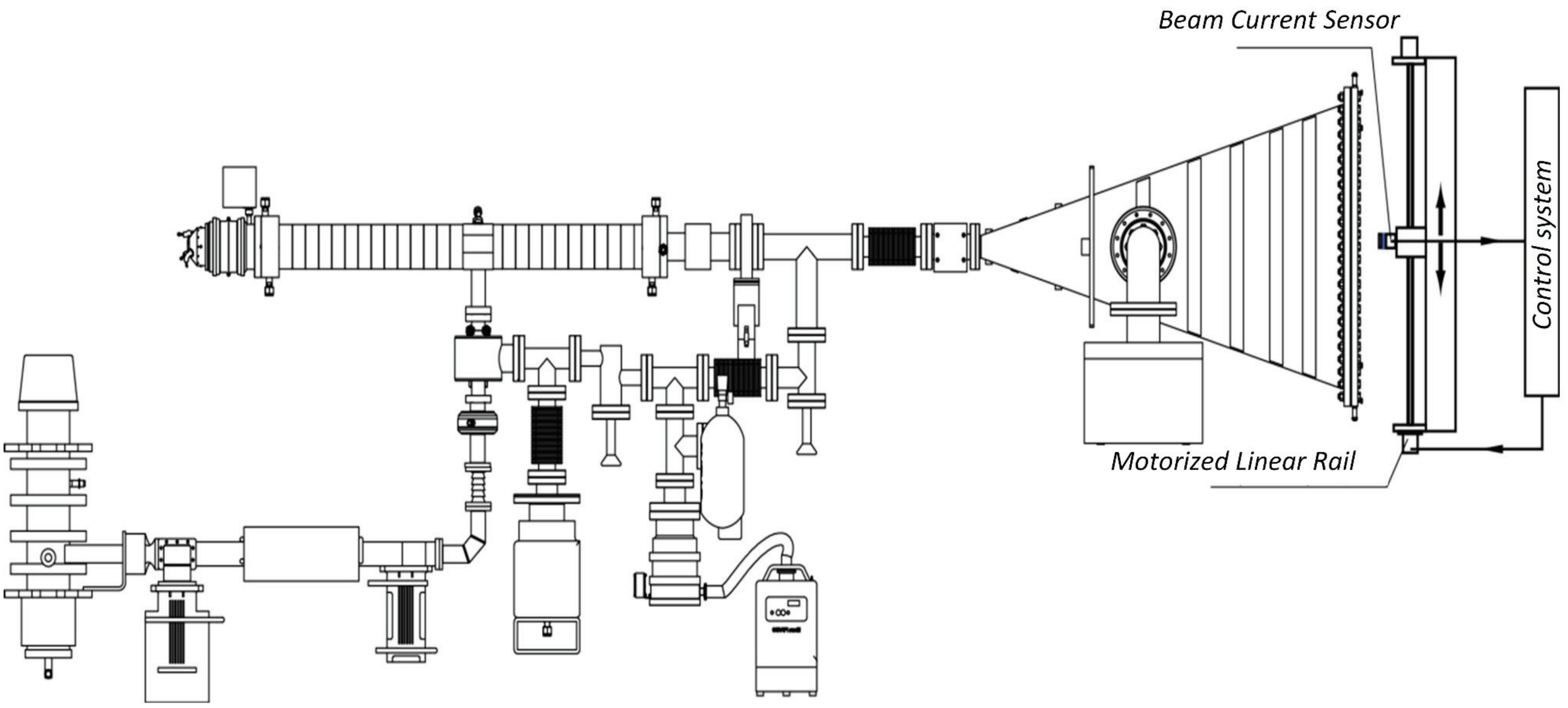

Figure 16: The measurements circuit of scanning system unevenness.

Beam energy and power measurements

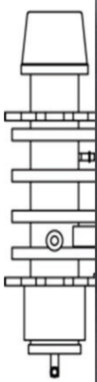

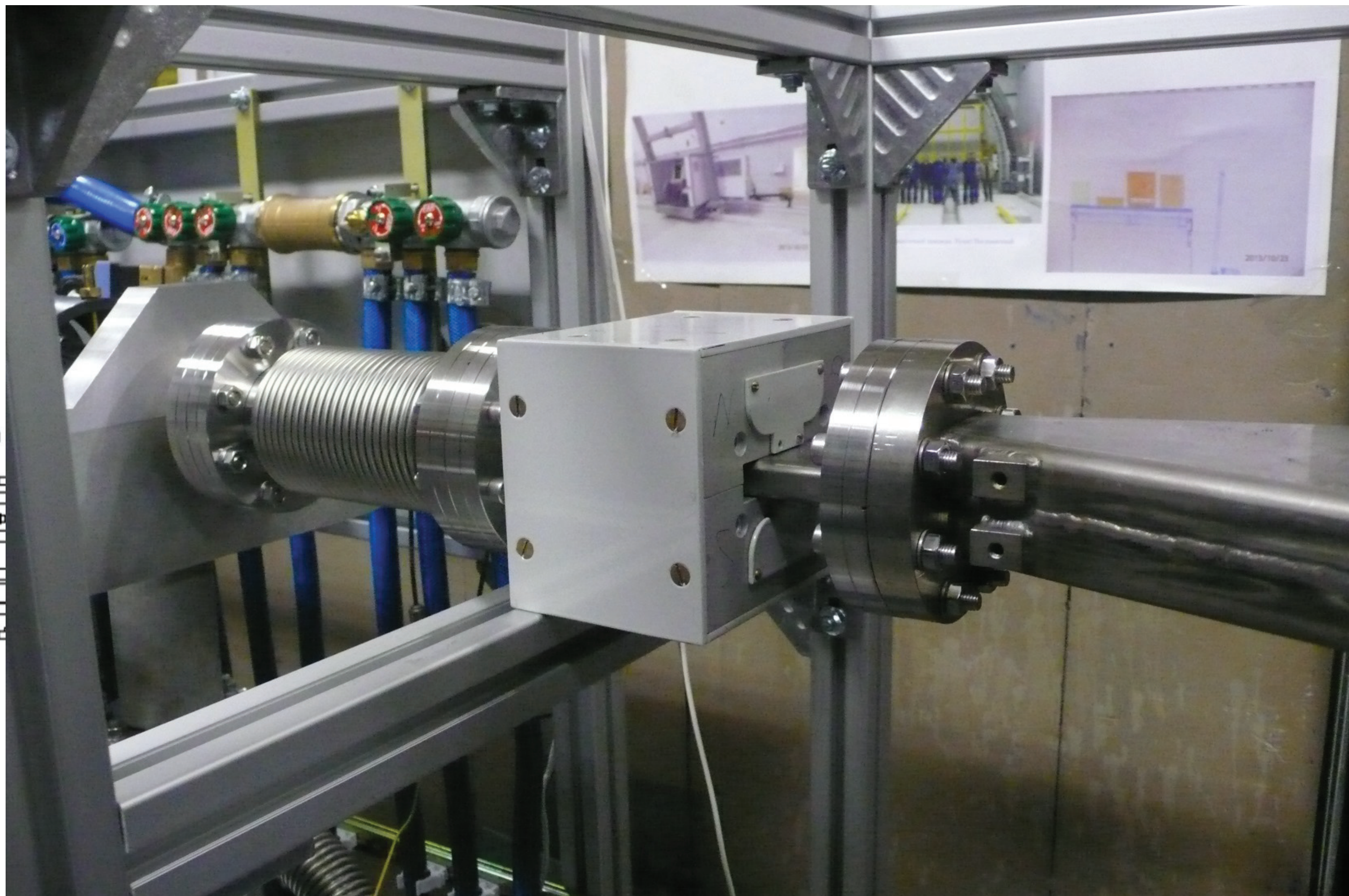

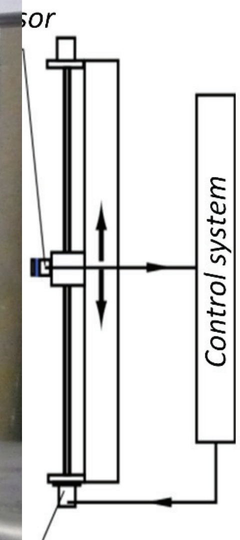

Figure

Beam energy and power measurements

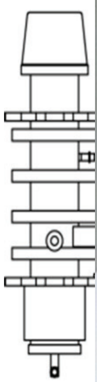

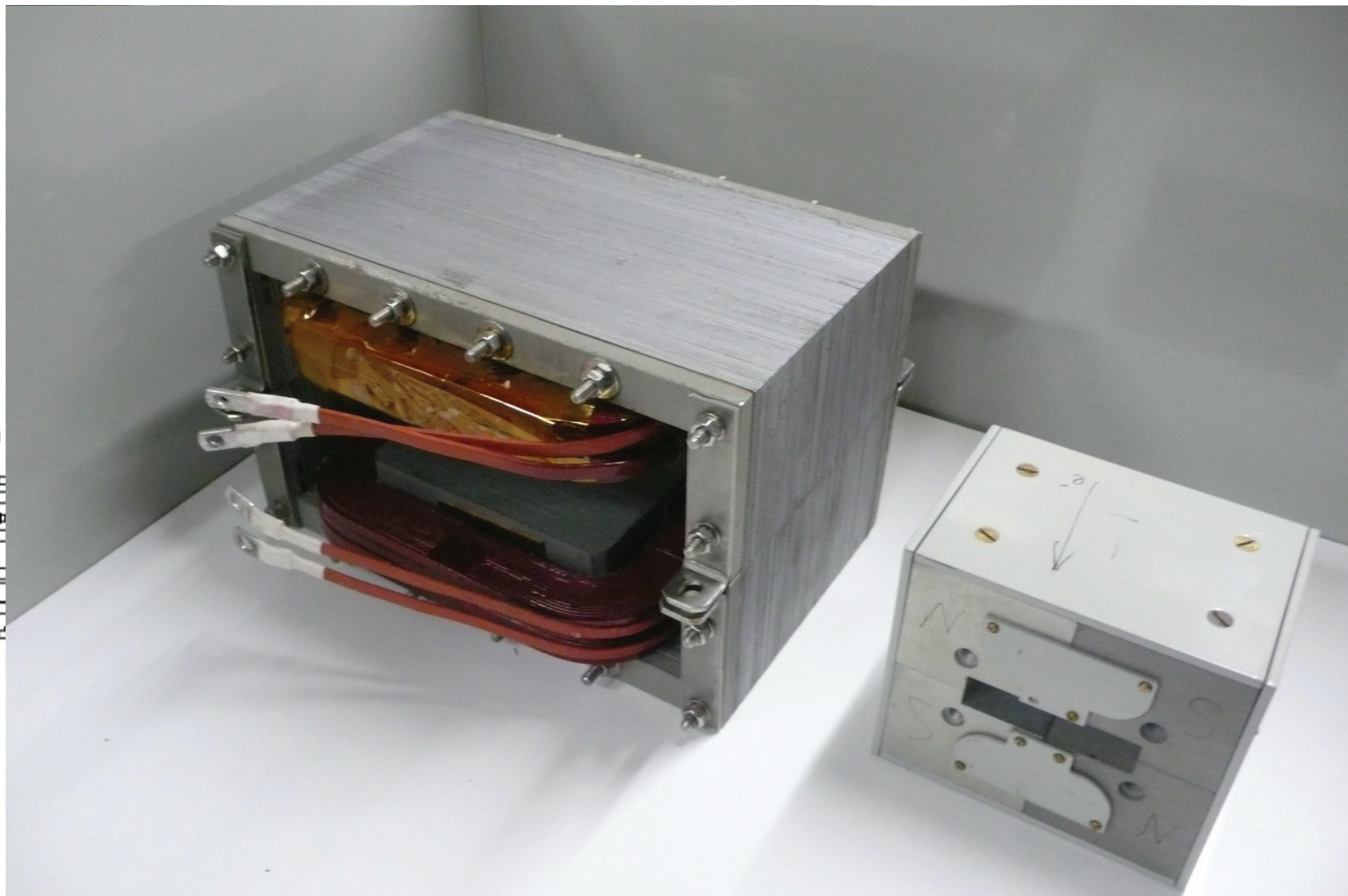

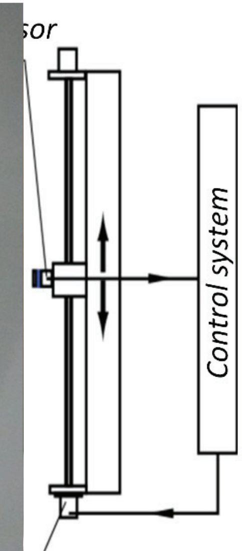

Figure

Measurements results

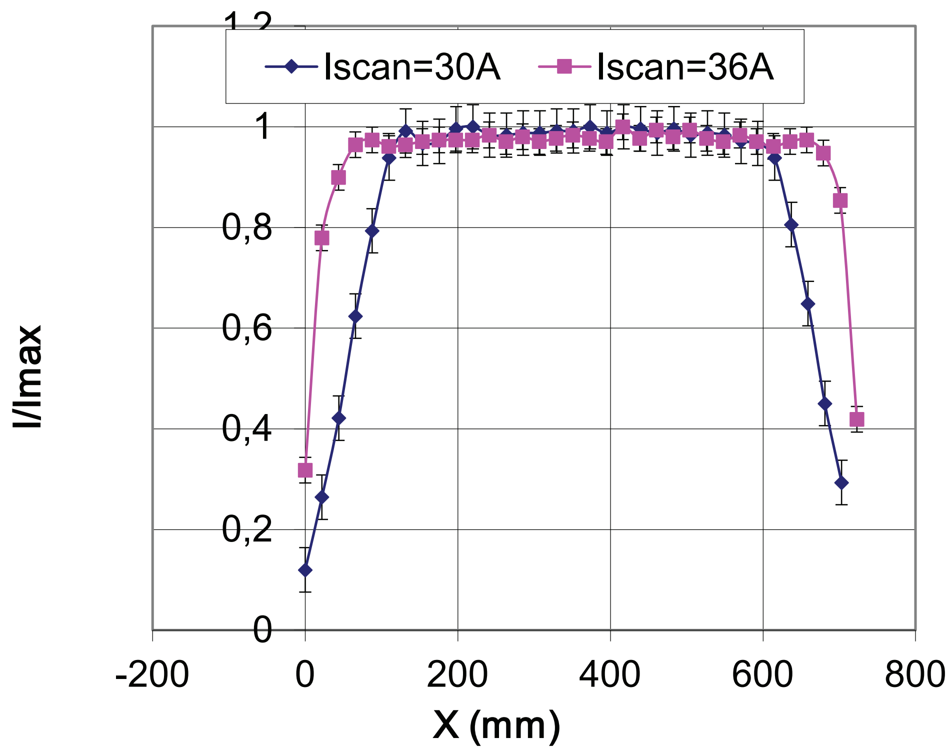

Figure 17: The beam current distribution at the electromagnetic scanner output.

Measurements results

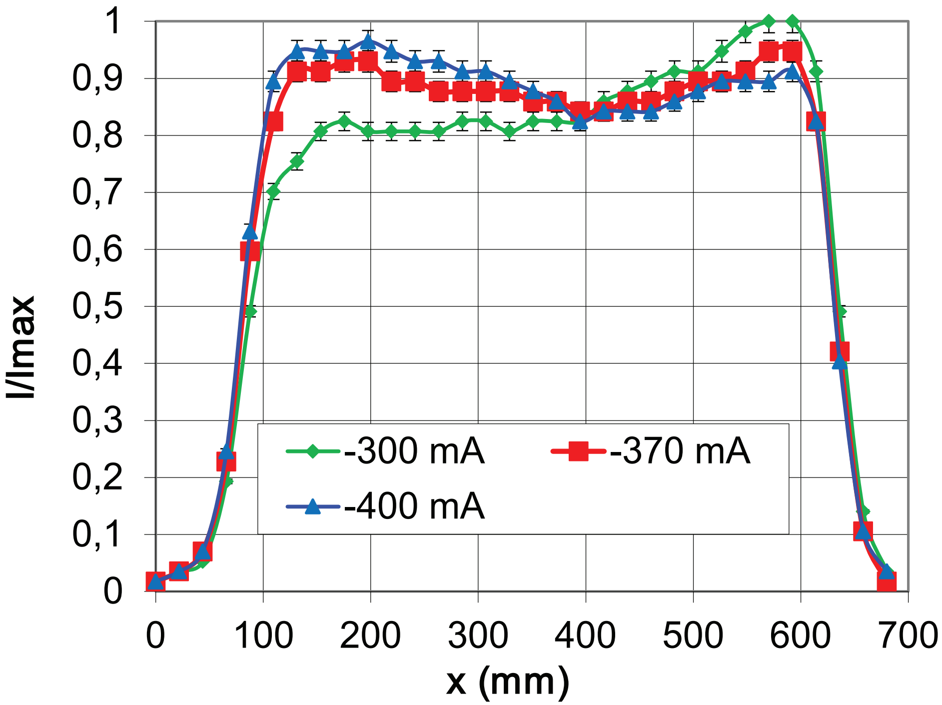

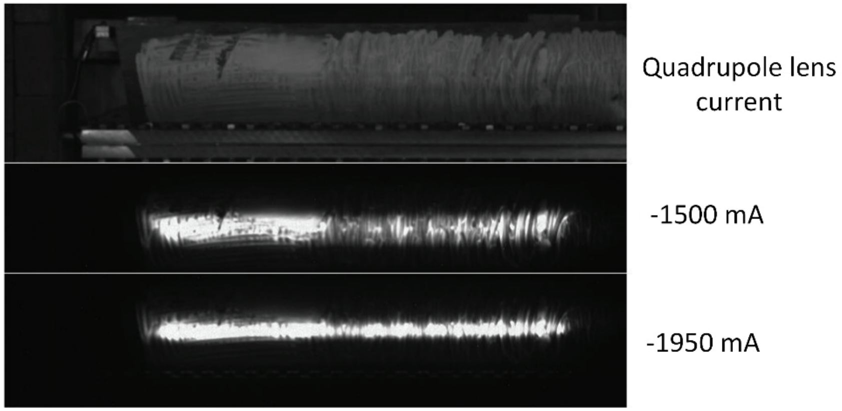

Figure 18: The beam current distribution at the scan chamber output. The nonlinear REPM lens forms the magnetic field.

SINP MSU

THANKS